JOURNAL OF SPACECRAFT AND ROCKETS
Vol. 29, No. 3, May–June 1992

Earth Aerobraking Strategies for Manned Return from Mars

Robert D. Braun* and Richard W. Powell*
NASA Langley Research Center, Hampton, Virginia 23665
and
J. Evans Lyne†
Eloret Institute, Palo Alto, California 94303

Earth-return entry corridor analyses are performed to evaluate the atmospheric flight environment of manned return from Mars. Trajectory and performance differences between aerocapture and direct entry are assessed and quantified in terms of the required aerobrake lift-drag ratio (L/D), stagnation-point heating, and the significance of off-nominal atmospheric conditions. The Earth-return aerobraking scenarios compared are 1) aerocapture into a phasing orbit with a 24-h period, 2) aerocapture into a 500-km circular orbit, 3) and direct entry to splashdown. No significant differences between aerocapture to a 500-km circular orbit and direct entry were observed in terms of aerobrake L/D requirements, maximum deceleration, or peak stagnation-point heat rate. The importance of parking orbit selection is demonstrated for low entry velocity Earth-return missions from Mars and missions returning from the Moon. Additionally, a stagnation-point heating analysis revealed that in all cases the peak heat rate is large enough to require an ablative thermal protection system for manned return from Mars. However, for entry velocities of 12.5 km/s and less, the heating environment is of the same order of magnitude as that experienced during the Apollo program. To perform the entry analysis, two predictor-corrector guidance design strategies were developed. Use of a predictor-corrector technique was shown to provide adequate flight margin for managing off-nominal atmospheric conditions.

Nomenclature

A	= reference surface area, m^2
C_D	= drag coefficient
g	= gravitational constant, 9.806 m/s^2
L/D	= lift-to-drag ratio
m	= vehicle mass, kg
m/C_DA	= ballistic coefficient, kg/m^2
$\dot{q}_c$	= convective stagnation-point heat rate, W/cm^2
$\dot{q}_r$	= radiative stagnation-point heat rate, W/cm^2
q_{tot}	= total stagnation-point heat load, J/cm^2
$\dot{q}_{tot}$	= total stagnation-point heat rate, W/cm^2
V_{atm}	= inertial velocity at the atmospheric interface, km/s
α	= angle of attack
ΔV	= propulsive velocity change, m/s
$\Delta\gamma$	= flyable corridor width, deg
γ_{atm}	= inertial flight-path angle at the atmospheric interface, deg
ρ	= atmospheric density, kg/m^3
ρ_{76}	= 1976 standard atmospheric density, kg/m^3

Introduction

Background and Objectives

WITH renewed interest in manned planetary exploration, NASA is currently analyzing the feasibility of a manned mission to Mars in the early 21st century. Because of the high transportation costs of launching to low Earth orbit (LEO), much of the mission feasibility hinges on the cost of transporting the vehicle to LEO. This cost is difficult to determine at this phase of the studies, but one major driver is the total mass that must be delivered. One method for reducing the required initial LEO vehicle mass is to employ aerobraking rather than retropropulsion to decelerate the spacecraft on arriving at Mars and returning to Earth. Aerobraking is defined as the deceleration resulting from the effects of atmospheric drag on a vehicle; thus, aerobraking eliminates the retropropulsion requirements for orbital capture, greatly reducing the amount of propellant needed. In comparison with an all-propulsive chemically propelled vehicle, aerobraking on arriving at Mars and returning to Earth has been shown to yield an initial mass reduction of 20–60%.[1] For an interplanetary mission that uses aerobraking, entry corridor analyses are required to insure that precisely enough energy is dissipated such that the vehicle makes a transition from its hyperbolic entry path to either the desired parking orbit or a direct entry trajectory.

In this investigation, Earth-return entry corridor analyses are performed to evaluate the atmospheric flight environment of manned return from Mars. The major emphasis of this research is to identify and quantify the effect that various atmospheric exit conditions have on the mission. Hence, the differences between aerocapture to a specific orbit and direct entry to a target splashdown site are investigated. Differences are quantified in terms of the aerobrake lift-drag ratio (L/D) requirements, stagnation-point heating, and the significance of off-nominal atmospheric conditions. In addition, the evolution of a direct entry guidance methodology from an aerocapture strategy is discussed. Three different Earth-return aerobraking scenarios are compared: 1) aerocapture into a phasing orbit with a 24-h period, 2) aerocapture into a 500-km circular orbit, 3) and direct entry to splashdown.

Vehicle Concepts and Earth-Return Options

In many recent studies that include high-energy aerobraking at Earth-return, low L/D configurations similar to the shapes of Apollo or the Aeroassist Flight Experiment (AFE) have been analyzed.[2] While providing adequate packaging volume, these vehicle concepts provide limited control authority during atmospheric flight. Additionally, radiative heating becomes a

Received Aug. 1, 1991; presented as Paper 91-2873 at the AIAA Atmospheric Flight Mechanics Conference, New Orleans, LA, Aug. 12–14, 1991; revision received Dec. 16, 1991; accepted for publication Dec. 17, 1991.

*Aerospace Engineer, Vehicle Systems Branch, Space Systems Division.
†Research Scientist.

significant concern for these blunt Earth-return configurations at the high entry velocities associated with interplanetary flight. One way to alleviate these problems is to select a more slender Earth-return shape that increases the hypersonic L/D and reduces the nose radius. However, slender, higher L/D vehicles are generally more difficult to package, while maintaining the proper center-of-gravity placement, and typically result in a higher ballistic coefficient.[3] As discussed in Ref. 2, minimizing the ballistic coefficient (hence, minimizing L/D) is desirable from an aerothermodynamic standpoint. Therefore, the approach employed in this investigation is to identify the minimum aerobrake L/D that yields enough control authority to be adequate for returning to Earth from Mars.

A few candidate vehicle shapes are presented in Fig. 1. These configurations, which have been studied in previous Earth-return analyses,[2,4,5] are representative of the relatively small capsule-like vehicle that the crew would enter shortly before Earth-return (because the wake region suitable for packaging the AFE derivative decreases with increasing L/D, this vehicle may only be a candidate for those missions requiring an L/D less than 0.3). In this manner, a majority of the interplanetary vehicle is discarded (including the habitation modules for the interplanetary flight) with only the crew and scientific cargo returning to Earth. This type of Earth-return mode, in which the emphasis is to place a crew on Mars and return them safely, is characteristic of the initial exploration scenarios emphasized in the recently released Stafford report.[6] In this analysis, the crew-return capsule is characterized by a 5-m base diameter, a mass of 6820 kg, and a ballistic coefficient of 310 kg/m^2. For comparison, Refs. 7–9 state that the Apollo command module had a base diameter of approximately 3.9 m, a entry mass of 5230 kg, and a ballistic coefficient of approximately 370 kg/m^2.

The three Earth-return mission modes selected for comparison in this analysis were chosen to span the broad range of options currently under study.[5,10-12] In the first option, the vehicle aerocaptures into a 24-h period phasing orbit (with a periapsis altitude of 500 km).[10] In this manner, orbital capture is insured, but the energy loss requirements of the aerocapture maneuver are minimized. However, other issues such as multiple passage through the Van Allen radiation belts and the addition of a propulsive stage to transfer from this highly elliptic phasing orbit to the space station must be considered. In the second option, the aerocapture maneuver provides a more significant deceleration such that the vehicle inserts directly into a LEO for space station rendezvous. This Earth-return mode is the typical choice of mission planners.[2,11,12] In the final Earth-return option, a direct-entry maneuver is performed,[5] and the mission ends with a parachute-braked, ocean splashdown. Although this scenario avoids the rendezvous issues associated with return to the space station (e.g., the additional mission requirement of orbital plane alignment), concerns pertaining to biological decontamination and a water recovery have to be addressed.

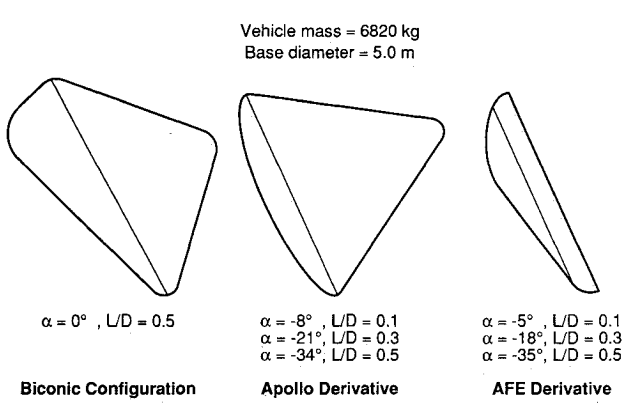

Fig. 1 Earth-return vehicle concepts.

Entry Corridor Definition

Interplanetary transfer analyses have shown that a wide range of aerobraking mission possibilities exists with Earth-entry velocities in the range of 11.5–14.0 km/s.[13] For a particular entry velocity, a lifting vehicle may follow one of numerous potential atmospheric trajectories while still achieving the desired atmospheric exit conditions; the difference in each of these transfers is the orientation of the vehicle lift vector and atmospheric interface flight-path angle γ_{atm}. For the case of aerocapture into a specified parking orbit, if too steep an atmospheric pass is flown, the vehicle will dissipate more energy than required and may not reach atmospheric exit. On the other hand, if the atmospheric flight is too shallow, the vehicle will exit with more energy than the parking orbit requires and may not capture. These bounding flight paths lead to the definition of an aerodynamic entry corridor as the set of all lift-modulated trajectories that yield the proper final state conditions.

As shown in Fig. 2, the upper bound of the aerodynamic corridor, which is achieved by flying the vehicle in a lift-down attitude, is the shallowest trajectory that the vehicle is able to fly while still achieving the proper energy decrement. In this manner, the vehicle stays in the atmosphere as long as possible, decelerating at a nearly constant altitude. Hence, the required energy loss, deceleration, and heat transfer are spread out over time. The lower corridor bound, which is attained by flying the vehicle in a lift-up attitude, is the steepest trajectory that still obtains the proper atmospheric exit conditions. By following this atmospheric flight path, the vehicle passes in and out of the atmosphere in the shortest amount of time. Because this trajectory must lose the same amount of energy as the lift-down transfer but in a shorter duration, it is characterized by a higher maximum deceleration and heating rate. The flyable entry corridor is defined as the aerodynamic corridor reduced by vehicle design considerations (e.g., a deceleration or heating limit). In this analysis, a peak deceleration limit of 5 g (where 1 g is equivalent to 9.806 m/s^2) was imposed. Hence, as shown in Fig. 2, the flyable corridor contains the subset of trajectories from within the aerodynamic corridor that do not exceed a peak 5-g deceleration. In a direct-entry scenario, corridor definition follows in an analogous manner with the bounds being specified by the atmospheric-skip-out and deceleration-limited transfers.

In an aerobraking performance analysis, one figure of merit is corridor width. This parameter is a measure of the aerodynamically induced control the vehicle may exert over its atmospheric flight path. In this analysis, corridor width is specified by the variance in the bounding inertial flight-path angles at the atmospheric entry interface (122-km altitude). To insure mission success, the width of the flyable entry corridor must be large enough to compensate for the uncertainties associated with the flight. In the case of a manned return from Mars,

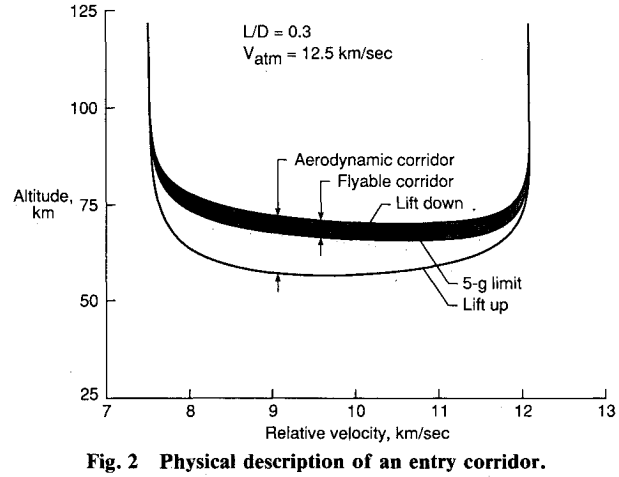

Fig. 2 Physical description of an entry corridor.

these mission uncertainties include initial state errors due to limitations of the interplanetary navigation system, as well as potential deviations in the atmospheric flight resulting from atmospheric uncertainties, mispredicted aerodynamics, and midcourse correction errors. For Earth-return from Mars, typical corridor width requirements are approximately 0.5–0.7 deg.[14]

Analysis Techniques

The entry corridor analysis was performed with the three-degree-of-freedom version of the Program to Optimize Simulated Trajectories (POST).[15] Within POST, the equations of motion are numerically integrated, and the targeting procedure uses numerically obtained partial derivatives. Two predictor-corrector atmospheric guidance algorithms were used in this analysis by including a three-degree-of-freedom simulation as an inner loop to the main simulation. The predictor-corrector algorithms were utilized to expand the flyable entry corridor by predicting and reducing high deceleration levels through bank-angle modulation. Additionally, the capability to manage off-nominal atmospheric conditions was evaluated.

For the cases of aerocapture into a specified orbit, a modified version of the guidance algorithm developed in Ref. 16 was employed. The guidance strategy utilized bank-angle modulation to control the exit energy and peak deceleration. Furthermore, roll reversal logic was included to insure the proper orbital plane (both longitude of ascending node and inclination) upon atmospheric exit. The models used by the predictor-corrector algorithm assumed instantaneous roll angle modulation, but the primary simulation modeled finite roll rates that were limited to a maximum of 15 deg/s. Upon completion of the aerocapture maneuver, propulsive burns are performed at apoapsis to raise the periapsis out of the atmosphere and then at periapsis to compensate for the apoapsis errors resulting from off-nominal atmospheric conditions (see Fig. 3). In the ensuing atmospheric dispersion analysis, the ΔV required to accomplish these two maneuvers is used as a figure of merit in evaluating the capability of a predictor-corrector guidance algorithm to manage off-nominal atmospheric events, the significance of precise atmospheric knowledge, and general mission viability.

For the case of direct entry to splashdown, a derivative of the algorithm based on Ref. 16 was also developed. From atmospheric entry to pull-up, the direct entry guidance strategy is the same as for the aerocapture Earth-return modes. In this manner, load relief was properly managed. Beyond the pull-up point, closed-loop linear feedback logic was utilized to establish constant altitude flight through bank-angle modulation. Once orbital capture was insured, ranging and azimuth calculations to the specified splashdown site were enabled. These splashdown site range and azimuth values were used by the second phase of the predictor-corrector logic. This guidance phase was responsible for determining the roll orientation history required to reach a specified parachute deployment point (at an altitude of 2300 m). This second phase of predictor-corrector control was typically established at a relative velocity of 6.5 km/s and an altitude of 60–65 km. Note that, once ranging predictor-corrector control was established, phugoidal oscillations were no longer damped. However, due to the relatively low energy remaining, these oscillations were generally minor. The ranging predictor-corrector was commanded to relinquish trajectory control as the relative velocity passed below 1 km/s at approximately 30 km. Beyond this point, the vehicle was guided by a closed-loop azimuth system, such that it was always headed toward the prescribed splashdown site. This azimuth system was employed until parachute deployment. Note that, although the direct-entry simulation begins hypersonically and concludes with a subsonic, parachute-braked splashdown, no Mach number or altitude effects were included in the vehicle aerodynamics.

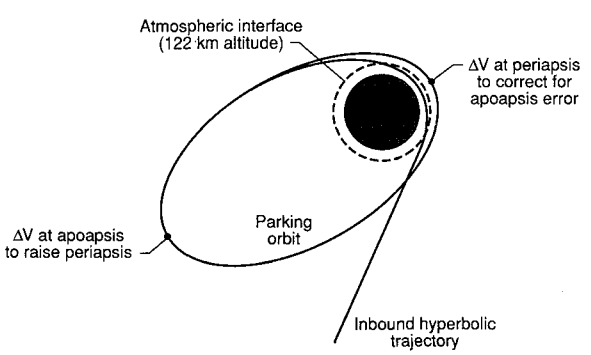

Fig. 3 Earth-return mission profile.

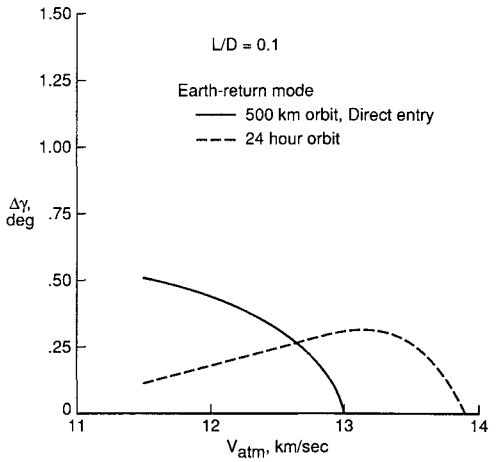

Fig. 4 Flyable corridor width for an aerobrake L/D of 0.1.

Convective stagnation-point heating was computed with use of the Sutton-Graves equation.[17] This equation is an approximate correlation developed from numerically obtained stagnation-point boundary-layer solutions for flows in chemical equilibrium over a range of flight conditions. Radiative stagnation-point heating was computed based on the tables provided by Sutton and Hartung in Ref. 18. These tables, which give the stagnation-point radiative heat rate as a function of freestream velocity, freestream density, and an effective nose radius, were utilized in a logarithmic interpolation routine to calculate the radiative heat rate along the trajectory. Throughout this paper, cold-wall heating values with no ablation are presented.

Results and Discussion

L/D Requirements

The flyable corridor width for an Earth-return vehicle with hypersonic L/D of 0.1 is presented in Fig. 4 as a function of entry velocity. Data for all three Earth-return modes is presented; however, the difference between aerocapture into a 500-km circular orbit and direct entry is undiscernible. For the case of aerocapture into a highly elliptic orbit, the flyable corridor width initially increases with entry velocity until the full lift-up boundary reaches the imposed deceleration limit (5 g). This occurs at approximately 13 km/s where the flyable corridor width is 0.32 deg. As the entry velocity increases beyond 13 km/s, the flyable corridor width is reduced significantly as a result of the restrictive effect of the deceleration limit. In fact, a flyable corridor does not even exist for entry velocities above 13.9 km/s. The restrictive influence of a deceleration constraint is further seen in the curves for the case of aerocapture into a 500-km circular orbit and direct entry. Even for the lowest Earth-return velocities, the increased energy decrement required and the use of such a low L/D aerobrake causes the corridor to be limited by a 5-g transfer. Hence, the flyable corridor width continuously decreases with increasing entry velocity until no feasible trajectories remain

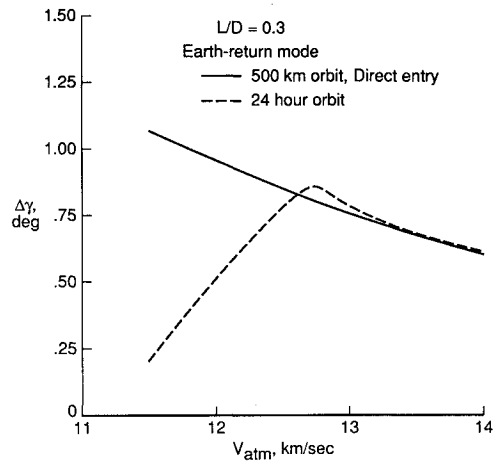

Fig. 5 Flyable corridor width for an aerobrake L/D of 0.3.

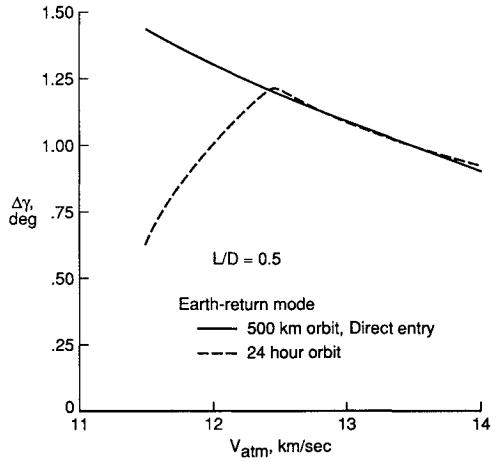

Fig. 6 Flyable corridor width for an aerobrake L/D of 0.5.

for entry velocities above 13 km/s. Finally, note that, regardless of the entry velocity or Earth-return mode, the corridor width does not approach that required to account for all of the potential mission uncertainties (0.7 deg); thus, more aerodynamic control authority (higher L/D) is required.

Figures 5 and 6 present the flyable corridor width as a function of entry velocity and Earth-return mode for vehicles with hypersonic L/D of 0.3 and 0.5, respectively. Similar trends to those discussed in relation to Fig. 4 are shown in these two figures; however, through use of a higher L/D vehicle, the corridor widths have substantially increased. Once again, in terms of the flyable corridor width, little difference between aerocapture into a 500-km circular orbit and direct entry is observed. Also, as in Fig. 4, Earth-return aerocapture into a highly elliptic parking orbit results in a corridor width curve that initially increases with entry velocity, reaches a maximum value where the full lift-up transfer reaches the 5-g limit, and then decreases with increasing entry velocity. On the other hand, aerocapture into a 500-km circular orbit or direct entry results in a flyable corridor that is restricted by the deceleration limit over the entire range of entry velocities considered. Thus, with increasing entry velocity, a continuously decreasing corridor width results. Although an aerobrake L/D of 0.3 appears to be feasible ($\Delta\gamma > 0.7$ deg) over a range of conditions (12.4–13.4 km/s for aerocapture into a 24-h orbit and 11.5–13.4 km/s for aerocapture into a 500-km circular orbit or the direct entry case), a slightly higher L/D is required to capture at the higher entry velocities. Based on the results of Fig. 6, an L/D of 0.5 appears to be more than adequate at entry velocities as high as 14 km/s where corridor widths of approximately 0.9 deg are observed. However, if the entry velocity were to increase above 14 km/s, entry analysis considerations would require a higher L/D vehicle than 0.5.

One additional result is implied in Figs. 4–6. In each figure, at the lower entry velocities, greater corridor width is obtained as the exit orbit becomes more circular. This increase in corridor width results from greater control authority being achieved through the requirement of a larger energy decrement. However, at the higher entry velocities where the flyable corridor is deceleration bounded, exiting into a more elliptic orbit is generally advantageous. For example, in Fig. 4, at 13.5 km/s, aerocapture into a 500-km circular orbit or direct entry is not possible without violating the imposed deceleration constraint; hence, the energy decrement must be relaxed (the exit orbit selected must be more elliptic). Additionally, at the higher entry velocities where the flyable corridor is deceleration bounded, the full lift-down boundary provides the only control over the flyable corridor width. This transfer becomes more shallow (resulting in a slightly greater corridor width) as the vehicle exits into a more elliptic parking orbit.

For a given L/D and entry velocity, an optimum parking orbit exists that yields the maximum control margin. This result is shown in Fig. 7, which depicts the effect of parking orbit selection on flyable corridor width. This figure demonstrates that parking orbit selection has a significant impact for the low entry velocity missions. This significance is only observed when the entry velocity is low enough such that parking orbit selection determines whether or not the corridor will be deceleration bounded. As a result, parking orbit selection is extremely important for the lunar mission with a return velocity of 11 km/s or low-energy Earth-return from Mars missions with entry velocities below 12 km/s. The influence of parking orbit selection on flyable corridor width is substantially reduced as the entry velocity is increased (above 12 km/s) since the corridor is necessarily deceleration bounded. However, parking orbit selection still retains some significance at the higher entry velocity conditions. Hence, to thoroughly optimize the Earth-return problem, parking orbit selection must be included, along with entry velocity, the deceleration limit, and the required corridor width, in determining the most promising Earth-return mission strategy.

Nominal Transfer Comparison

Based on the results presented in Fig. 6, an aerobrake L/D of 0.5 was selected as the minimum required L/D for the Earth-return maneuver. This selection is consistent with that made in Refs. 5 and 11. Nominal transfers that pass through the center of the flyable corridor were identified for each entry velocity/Earth-return mode combination for this aerobrake configuration. These transfers were then compared to assess the variance in atmospheric flight path, deceleration, heat rate, and heat load for the three Earth-return modes. Addi-

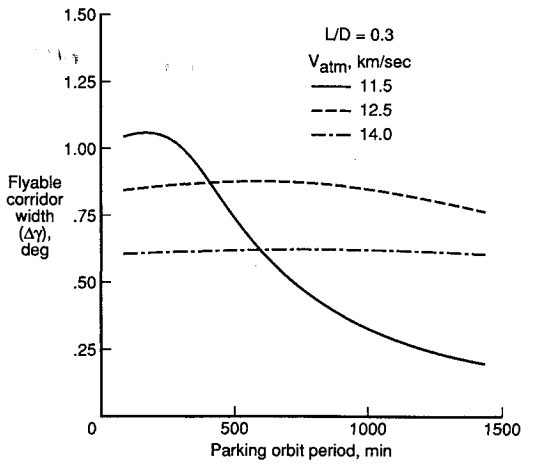

Fig. 7 Effect of parking orbit selection on flyable width.

tionally, these nominal transfers were utilized as a reference point in the predictor-corrector guidance design and atmospheric dispersion analysis.

Specification of the final state of the mission (exit orbital energy or a direct entry condition) has a significant impact on the aerobraking trajectory. Figures 8 and 9 illustrate the variation in altitude and deceleration histories, respectively, for the three Earth-return modes and a 14 km/s entry condition. Figure 8 shows that as the required final velocity decreases (requiring a larger energy decrement), the vehicle stays in the atmosphere longer; however, the pull-up altitude does not necessarily have to change. In fact, the three transfers are identical through pull-up, and the vehicle adjusts for the variance in exit state by modulating the post-pull-up portion of the transfer. As a result, the peak deceleration values (Fig. 9) are the same regardless of the Earth-return mode. However, the deceleration characteristics change from a relatively short duration spike to a longer, multiple-humped shape. Note that the final spike in the direct entry deceleration profile results from the parachute deployment. Also, as depicted in Fig. 8, the direct entry nominal transfer follows a constant-altitude path for a portion of the descent by employing a closed-loop linear-feedback guidance technique. Beyond this constant-altitude portion of flight, predictor-corrector guidance control is established and minor phugoidal oscillations are not damped, resulting in a multiple-humped deceleration profile (Fig. 9).

Stagnation point heating information for each of the nominal transfers is listed in Table 1 based on an effective nose radius of 3 m and a ballistic coefficient of 310 kg/m^2. These heating values that are illustrated for comparison purposes are representative of the nominal heating environment during manned return from Mars. However, thermal protection system design should be based on the more severe heating conditions that occur by following the full lift-up transfer. For each transfer, the convective and radiative contributions to the total peak heat rate are presented. Additionally, the total heat load is shown. From this table, no distinction exists (in terms of peak heat rate) between aerocapture to 500-km circular orbit and direct entry, regardless of entry velocity. This results from the transfers being identical through pull-up that typically occurs after the vehicle has passed through peak heating. Note that, in all cases, the peak heat rate is large enough to require an ablative thermal protection system for Earth-return from Mars.

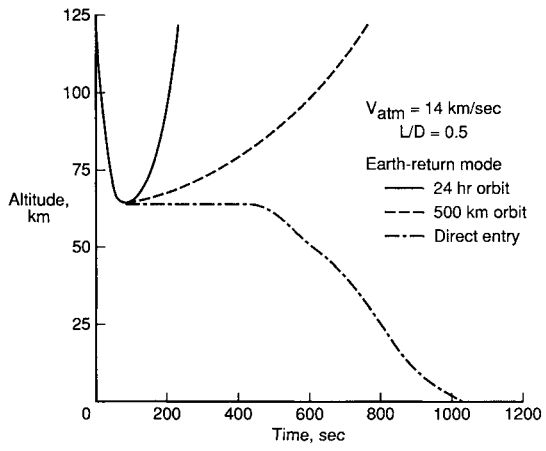

Fig. 8 Altitude history comparison for various Earth-return modes.

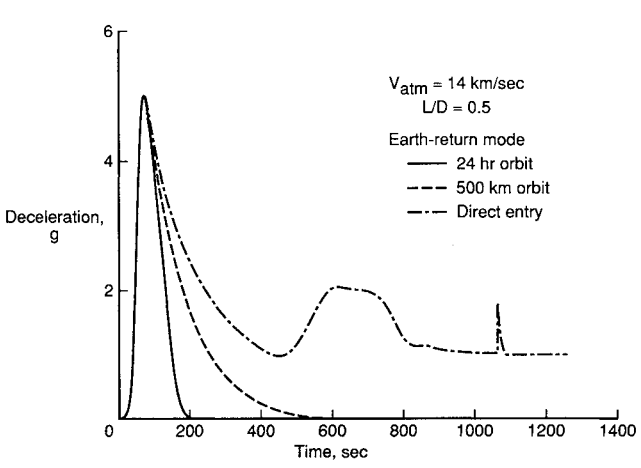

Fig. 9 Deceleration history comparison for various Earth-return modes.

Table 1 Heating during Earth return from Mars; m = 3 m, m/C_DA = 310 kg/m^2

V_{atm}, km/s	Earth-return mode	$\dot{q}_{c,max}$, W/cm^2	$\dot{q}_{r,max}$, W/cm^2	$\dot{q}_{tot,max}$, W/cm^2	q_{tot}, J/cm^2
11.5	24 h	107.5	73.0	180.5	1.3×10^4
	500 km	165.2	168.7	333.9	2.4×10^4
	Direct	165.2	168.7	333.9	3.0×10^4
12.5	24 h	189.2	366.3	555.5	3.0×10^4
	500 km	203.5	424.0	627.5	4.2×10^4
	Direct	203.5	424.0	627.5	5.0×10^4
14.0	24 h	271.9	887.0	1158.9	7.1×10^4
	500 km	271.9	887.0	1158.9	8.8×10^4
	Direct	271.9	887.0	1158.9	9.5×10^4

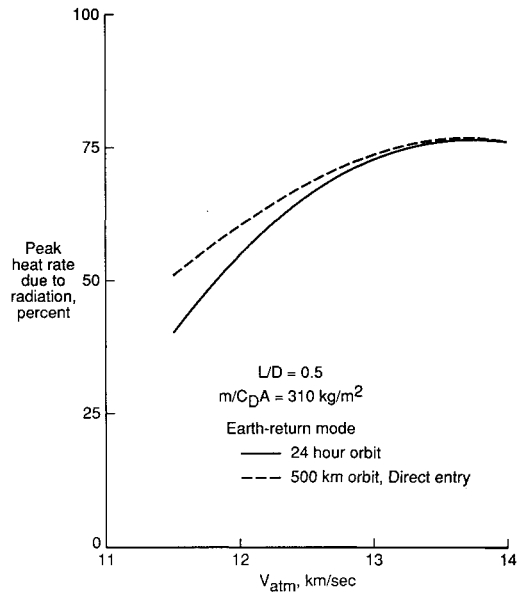

Fig. 10 Significance of radiative heating during Earth-return from Mars.

As shown in Table 1, a relatively minor distinction (in terms of the total heat load) is observed between aerocapture to a 500-km circular orbit and direct entry (with the direct entry case being higher). The percentage of the total peak heat rate due to radiation is shown in Fig. 10 for each nominal transfer. Depending on the entry velocity and Earth-return mode, radiation accounts for 40–77% of the total peak heat rate with the larger contributions corresponding to the higher entry velocity cases. For comparison, note that the Apollo command module endured a heat rate as high as 490 W/cm^2 and a total heat load as high as 4.3×10^4 J/cm^2 during the unmanned qualification flight of Apollo 4.[19] Less severe heating was encountered during the manned flights (Apollo 8 and 10–16) with a peak heat rate between 310–400 W/cm^2 and a total heat load between 2.9×10^4 and 3.2×10^4 J/cm^2 (Ref. 9). During these

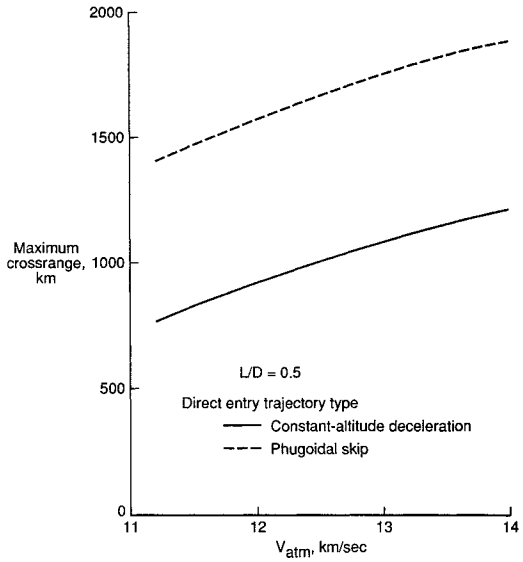

Fig. 11 Maximum available cross range for direct entry transfers.

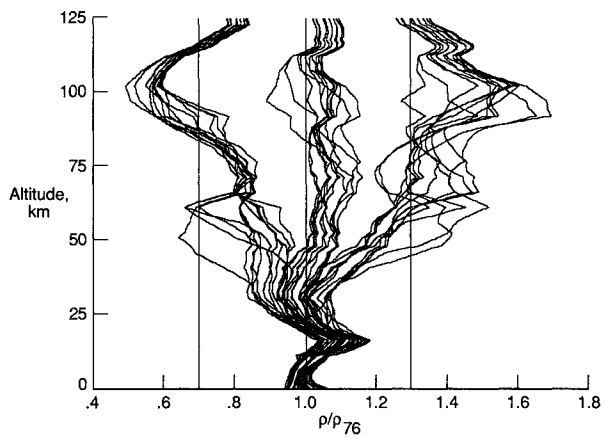

Fig. 12 Atmospheric density profiles used to direct entry simulations from atmospheric interface to touchdown.

flights, radiation contributed approximately 33% to the total peak heat rate.[20] Hence, the heating environment for manned return from Mars at entry velocities of 12.5 km/s and less is of the same order of magnitude as that experienced during the Apollo program.

Figure 11 presents the maximum available cross range for an Earth-return, direct-entry vehicle with L/D of 0.5 as a function of entry velocity. These cross-range values were obtained with and without the use of phugoidal skips to demonstrate the merit of such an entry strategy. The direct-entry strategy relied on an optimal bank angle history to roll in the direction of maximum cross range. Once the maximum cross-range azimuth is achieved, the vehicle is commanded to roll to a lift-up orientation to gain as much cross range as possible. As expected, the available cross range increases with increasing entry velocity from 830 km at 11.5 km/s to 1200 km at 14 km/s for the constant-altitude deceleration case. As shown in Fig. 11, by including phugoidal skip maneuvers (as in the Apollo program), a significantly greater degree of cross range could be achieved. However, the increased available cross range shown is slightly optimistic as a result of not including altitude effects in the aerodynamics. Due to the high entry velocities associated with manned return from Mars, the constant-altitude deceleration profiles provide more than adequate cross range and were selected to design the nominal direct-entry guidance strategy.

Atmospheric Dispersions Analysis

To evaluate the capability of the guidance algorithm to manage atmospheric density uncertainty and demonstrate the significance of off-nominal atmospheric effects, 36 atmospheric density and wind profiles were generated with use of the GRAM program.[21] These profiles, which are illustrated in Figs. 12 and 13, represent the mean and 3-σ maximum and minimum density profiles for each of the 12 months in the year 2020. Simulations were performed in which the Earth-return vehicle returning with an entry velocity of 14 km/s encountered each atmosphere; in these cases, the monthly mean density profile was used within the guidance loop as the expected density profile. Although the wind profiles illustrated in Fig. 13 were encountered in the simulation, the guidance algorithm was not given any wind knowledge. Also, note that, in this analysis, no horizontal density variation was included; that is, the density profiles were a function of altitude only. In addition, although the simulation begins with a hypersonic entry and concludes with a subsonic, parachute-braked splashdown, no Mach number or altitude effects were included in the vehicle aerodynamics (a constant L/D of 0.5 was assumed). However, once an available database exists, these effects could be easily incorporated in the simulation.

From a mission feasibility standpoint, the severity of these off-nominal atmospheric conditions can be assessed by considering either the required change in the postaerocapture ΔV (for the aerocapture to orbit cases) or splashdown site miss distance (for the case of direct entry). Figure 14 depicts the required ΔV change as a result of a mispredicted density profile for Earth-return aerocapture into a highly elliptic orbit. For comparison purposes, the nominal postaerocapture ΔV is 26.7 m/s. This figure shows that only a minor increase

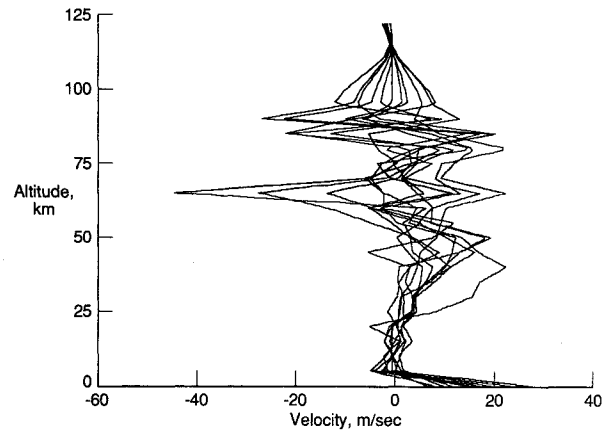

Fig. 13a North-south wind profiles used in direct entry simulations from atmospheric interface to touchdown.

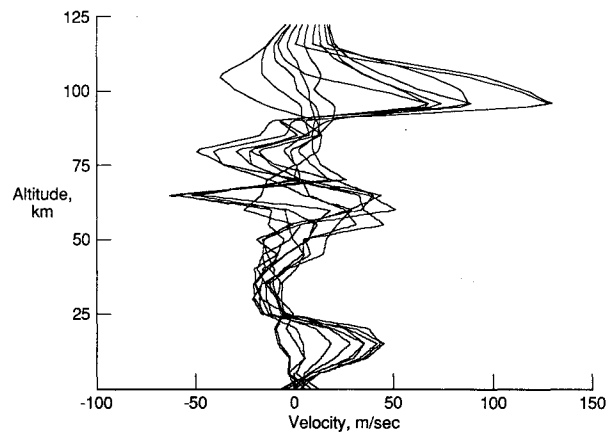

Fig. 13b East-west wind profiles used in direct entry simulations from atmospheric interface to touchdown.

in postaerocapture ΔV is required to account for the uncertainty in these density and wind models (the greatest increase being 6 m/sec). Inclusion of a drag-feedback system in the guidance algorithm is the major reason that such a small change in the postaerocapture ΔV is required. This system determines the error between the predicted and encountered drag forces and adjusts the guidance-loop density (altitude) to match the encountered value. Utilization of this feedback system is analogous to the use of onboard accelerometer measurements during flight.

Figure 15 depicts the required ΔV change as a result of a mispredicted density profile for Earth-return aerocapture into a 500-km circular orbit. For comparison, the nominal postaerocapture ΔV is 124.2 m/s. Once again, notice that only a relatively minor change in postaerocapture ΔV is required to account for these off-nominal effects (the greatest increase being 15 m/s). Additionally, note that, in a few cases, a mispredicted atmospheric density profile actually resulted in a lower ΔV requirement than the nominal case. This lower requirement is an artifact of the ΔV measurement being a sum total of two burns, one at apoapsis and one at periapsis. In the case of aerocapture to a 500-km circular orbit, the apoapsis burn (required to raise periapsis out of the atmosphere) is much larger than the periapsis burn (used to null out the apoapsis error that results from an off-nominal atmospheric prediction). When the vehicle flies through a significantly denser atmosphere than expected, the guidance system commands a lift-up attitude, and as a result the atmospheric exit periapsis is larger than the nominal periapsis; hence, a smaller periapsis-raise maneuver is required than in the nominal case. When this decrease in the periapsis-raise maneuver is larger than the increase in the apoapsis-trim maneuver, a negative ΔV change results. Hence, in some cases, it is actually advantageous (although, only slightly so with a maximum decrease of 2 m/s) to encounter an unexpected density profile.

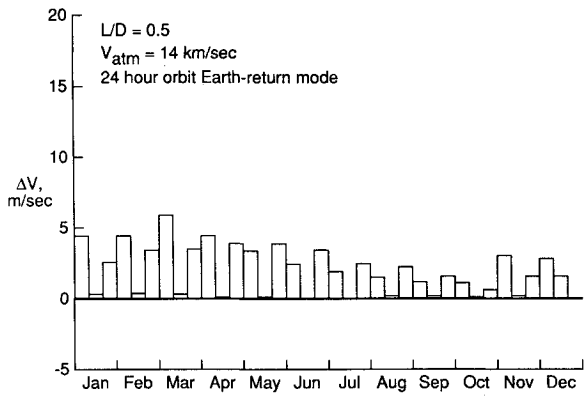

Fig. 14 Additional postaerocapture ΔV requirements resulting from off-nominal atmospheric effects (relative to a nominal ΔV of 26.7 m/s).

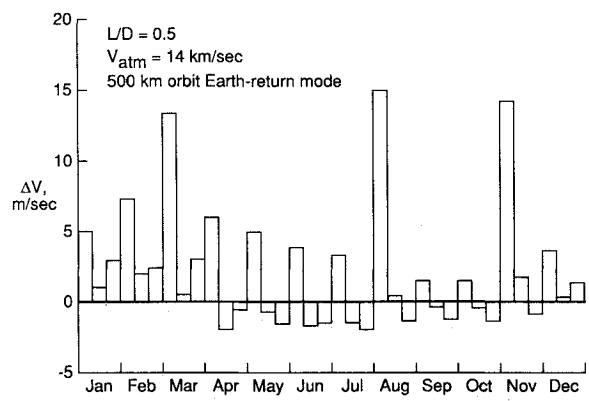

Fig. 15 Additional post-aerocapture ΔV requirements resulting from off-nominal atmospheric effects (relative to a nominal ΔV of 124.2 m/s).

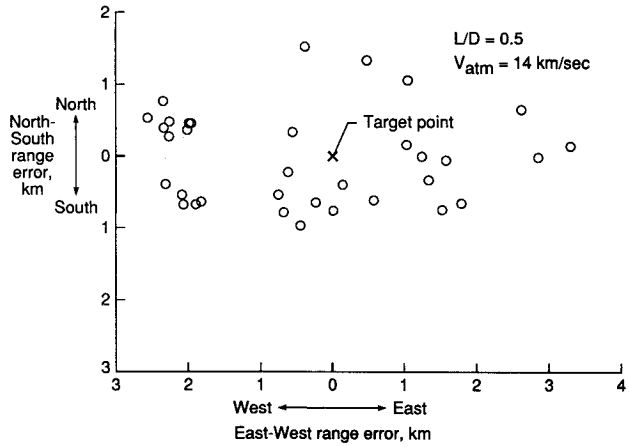

Fig. 16 Splashdown dispersion footprint.

Figure 16 illustrates the splashdown footprint for the 36 direct entry cases (the target splashdown point is also shown) and demonstrates the relatively high degree of precision that can be expected from the inclusion of a predictor-corrector guidance capability. The largest range error is approximately 3.5 km at splashdown. However, a majority of this error accumulates after the vehicle's relative velocity passes below 1 km/s and the ranging predictor-corrector has relinquished control to the closed-loop azimuth system. In fact, range errors at the time that the predictor-corrector is turned off were less than 0.1 km and the offset in the vehicle's position at the time of parachute deployment was typically less than 0.6 km. Hence, a majority of the splashdown error can be attributed to the effect of atmospheric winds on the parachute-braked portion of the entry in which the vehicle is in a state of free fall. Relative to the north-south range errors, the larger east-west splashdown errors shown in Fig. 16 can also be attributed to the magnitude of the low-altitude wind profiles (see Fig. 13) after parachute deployment. Hence, use of a predictor-corrector guidance technique provides adequate flight margin for managing off-nominal density and wind profiles.

Concluding Remarks

Through this investigation, Earth-return entry corridor analyses have been performed to evaluate the atmospheric flight environment of manned return from Mars. Trajectory and performance differences between aerocapture to a specific orbit and direct entry to a target splashdown site have been assessed and quantified in terms of the aerobrake lift-drag ratio (L/D) requirements, stagnation-point heating, guidance algorithm design, and the significance of off-nominal atmospheric conditions. The Earth-return aerobraking scenarios compared were 1) aerocapture into a phasing orbit with a 24-h period, 2) aerocapture into a 500-km circular orbit, 3) and direct entry to splashdown.

No significant differences were observed between aerocapture to a 500-km circular orbit and direct entry in terms of L/D requirements (flyable corridor width), peak deceleration, or stagnation-point heat rate. Furthermore, only a slightly higher total heat load was observed for the direct entry trajectories. Significant performance distinctions were observed with use of a more elliptic parking orbit (with a 24-h period) that required a lower energy decrement. These performance distinctions demonstrated the importance of including parking orbit effects in the mission design analysis, particularly for low-entry velocity Earth-return missions from Mars or missions returning from the Moon.

To span the entire range of entry velocities considered for manned return from Mars (11.5–14.0 km/s), an aerobrake

L/D of approximately 0.5 is required. However, an aerobrake L/D on the order of 0.3 is sufficient for a limited range of entry conditions (12.4–13.4 km/s for aerocapture into a 24-h orbit and 11.5–13.4 km/s for aerocapture into a 500-km circular orbit or the direct entry case). If entry velocities greater than 14.0 km/s are considered, an L/D greater than 0.5 is required. A stagnation-point heating analysis revealed that in all cases the peak heat rate is large enough to require an ablative thermal protection system for manned return from Mars. However, for the lower velocity entries, the heating environment is the same order of magnitude as that experienced during the Apollo program.

Although two guidance design strategies were employed in this analysis (one for aerocapture and another for direct entry), both algorithms are based on the predictor-corrector methodology. This technique demonstrated the capability to manage off-nominal atmospheric conditions extremely well. For the cases of aerocapture to a parking orbit, the maximum increase in the nominal postaerocapture ΔV was 15 m/s. Additionally, in some cases, flight through an off-nominal atmospheric profile resulted in a smaller than nominal postaerocapture ΔV. For the case of direct entry to splashdown, minimal splashdown range errors were observed (the largest error being 3.5 km). A majority of this range error accrues during the parachute-braked phase of flight in which the vehicle is unguided.

References

[1]Braun, R. D., Powell, R. W., and Hartung, L. C., "The Effect of Interplanetary Trajectory Options on a Manned Mars Aerobrake Configuration," NASA TP-3019, Aug. 1990.

[2]Walberg, G. D., "A Review of Aerobraking for Mars Missions," International Astronautical Federation, IAF Paper 88-196, Oct. 1988.

[3]Cruz, M. I., Armento, R. F., and Giles, W. H., "Aerocapture—A System Design for Planetary Exploration," International Astronautical Federation, IAF Paper 79-160, Sept. 1979.

[4]Syvertson, C. A., "Research Problems in Atmosphere Entry and Landing for Manned Planetary Mission," NASA TN D-4977, Jan. 1969.

[5]Tauber, M., Palmer, G., and Yang, L., "Earth Atmospheric Entry Studies for Manned Mars Missions," AIAA Paper 90-1699, June 1990.

[6]Anon., "America at the Threshold," Report of the Synthesis Group on America's Space Exploration Initiative, U.S. Government Printing Office, Washington, DC, May 1991.

[7]Hillje, E. R., "Entry Aerodynamics at Lunar Return Conditions Obtained from the Flight of Apollo 4 (AS-501)," NASA TN D-5399, Oct. 1969.

[8]Lee, D. B., and Goodrich, W. D., "The Aerothermodynamic Environment of the Apollo Command Module During Superorbital Entry," NASA TN D-6792, April 1972.

[9]Pavlosky, J. E., and St. Leger, L. G., "Apollo Experience Report—Thermal Protection Subsystem," NASA TN D-7564, Jan. 1974.

[10]Young, A. C., "Mission and Vehicle Sizing Sensitivities," NASA TM 89320, June 1986, pp. 87–102.

[11]Lyne, J. E., Tauber, M. E., and Braun, R. D, "Earth-Return from Mars," AIAA Paper 91-2874, Aug. 1991.

[12]Menees, G. P., "Aeroassisted-Vehicle Design Studies for a Manned Mars Mission," International Astronautical Federation, IAF/IAA Paper 87-433, Oct. 1987.

[13]Braun, R. D., "The Influence of Interplanetary Trajectory Options on a Chemically Propelled Manned Mars Vehicle," *Journal of Astronautical Sciences,* Vol. 38, No. 3, 1990, pp. 289–310.

[14]Willcockson, W. H., "OTV Aeroassist with Low L/D," *Acta Astronautica,* Vol. 17, No. 3, 1988, pp. 277–301.

[15]Brauer, G. L., Cornick, D. E., and Stevenson, R., "Capabilities and Applications of the Program to Optimize Simulated Trajectories (POST)," NASA CR-2770, Feb. 1977.

[16]Braun, R. D., and Powell, R. W., "A Predictor-Corrector Guidance Algorithm for Use in High-Energy Aerobraking System Studies," AIAA Paper 91-0058, Jan. 1991.

[17]Sutton, K., and Graves, R. A., Jr., "A Generalized Stagnation-Point Convective-Heating Equation for Arbitrary Gas Mixtures," NASA TR R-376, Nov. 1971.

[18]Sutton, K., and Hartung, L. C., "Equilibrium Radiative Heating Tables for Earth Entry," NASA TM 102652, May 1990.

[19]Lee, D. B., "Apollo Experience Report—Aerothermodynamics Evaluation," NASA TN D-6843, June 1972.

[20]Curry, D. M., and Stephens, E. W., "Apollo Ablator Thermal Performance at Superorbital Entry Velocities," NASA TN D-5969, Sept. 1970.

[21]Justus, C. G., Fletcher, G. R., Gramlina, F. E., and Pace, W. B., "The NASA/MSFC Global Reference Atmospheric Model—Mod 3 (with Spherical Harmonic Wind Model)," NASA CR-3256, 1980.

Ernest V. Zoby
Associate Editor